

A Study of Excited Ω_b^- States in Hypercentral Constituent Quark Model via Artificial Neural Network

Halil Mutuk*

*Physics Department, Faculty of Arts and Sciences,
Ondokuz Mayıs University, 55139, Samsun, Turkey*

In this work, we have obtained mass spectra, radiative decay widths and strong decay widths of newly observed excited Ω_b^- states, i.e. $\Omega_b(6316)^-$, $\Omega_b(6330)^-$, $\Omega_b(6340)^-$, and $\Omega_b(6350)^-$. Mass spectrum is obtained in Hypercentral Constituent Quark Model (hCQM) by solving six-dimensional nonrelativistic Schrödinger equation via Artificial Neural Network (ANN). In this respect, radiative decay widths are calculated by a generalization of a framework from meson to baryon. Also, strong decay widths of the low-lying Ω_b states within 3P_0 model are calculated. Obtained results are presented with the comparison of available experimental data and other theoretical studies.

I. INTRODUCTION

In the past years, significant experimental progress has been made in heavy baryon physics. In resemblance with the atomic spectroscopy, where transitions of the lines in the spectrum gives information about the interaction between the atomic core and the electrons, energy of the resonances gives information about interaction inside the nucleons. According to quark model, hadrons are strongly interacting particles that are made of quarks.

In this context, the heavy baryons have been got much attention theoretically and experimentally in the last decade. Single heavy baryon system (Qqq) is composed of a heavy (Q) quark and two light quarks (qq) which is bound via gluon interactions. This system is the QCD analogue of the helium atom in which two electrons (light particles) are orbiting around a fixed proton (heavy particle) bounded by the electromagnetic interactions.

Very recently, the LHCb collaboration reported four narrow peaks in the $\Xi_b^0 K^-$ mass spectrum [1]

$$\begin{aligned} \Omega_b(6316)^- : M &= 6315.64 \pm 0.31 \pm 0.07 \pm 0.50 \text{ MeV}, \\ \Gamma &< 2.8 \text{ MeV} \end{aligned} \quad (1)$$

$$\begin{aligned} \Omega_b(6330)^- : M &= 6330.30 \pm 0.28 \pm 0.07 \pm 0.50 \text{ MeV}, \\ \Gamma &< 3.1 \text{ MeV} \end{aligned} \quad (2)$$

$$\begin{aligned} \Omega_b(6340)^- : M &= 6339.71 \pm 0.26 \pm 0.05 \pm 0.50 \text{ MeV}, \\ \Gamma &< 1.5 \text{ MeV} \end{aligned} \quad (3)$$

$$\begin{aligned} \Omega_b(6350)^- : M &= 6349.88 \pm 0.35 \pm 0.07 \pm 0.50 \text{ MeV}, \\ \Gamma &= 1.4_{-0.8}^{+1.0} \pm 0.1 \text{ MeV}, \end{aligned} \quad (4)$$

where the uncertainties are statistical, systematic and the last is due to the knowledge of Ξ_b^0 mass. The significances of these states are 2.1σ for $\Omega_b(6316)^-$, 2.6σ and exceed 5σ for $\Omega_b(6340)^-$ and $\Omega_b(6350)^-$.

Before the LHCb's measurement there is a vast literature for the mass spectrum of the excited Ω_b states by various quark models [2–7], QCD Sum Rules [8–12] and Regge phenomenology [13–15]. The experimental result

has already stimulated theoretical works. In Ref. [16], Chen et al. systematically studied the internal structure of P -wave Ω_b baryons, and calculated their mass spectra and strong decay properties by QCD Sum Rules method. They concluded that all the four excited Ω_b baryons recently discovered by LHCb can be well explained as P -wave Ω_b baryons. In Ref. [17], Liang and Lü studied the strong decays of the low-lying Ω_b states within the 3P_0 model and pointed out that these excited states can be reasonably assigned as λ -mode $\Omega_b(1P)$ states. The possible interpretations of the four peaks as the meson-baryon molecular states were studied by Liang and Oset [18]. They claimed four states at higher energies which are seen as peaks with the same statistical significance as the first of the states claimed. Wang used explicit P -wave between the two s -quarks to construct the current operators to study the P -wave Ω_b states with the full QCD sum rules by carrying out the operator product expansion up to the vacuum condensates of dimension 10 [19]. Xiao et al. elaborated OZI allowed two-body strong decays of the low-lying λ -mode Ω_b baryons up to $N=2$ shell using the chiral quark model within the $j-j$ coupling scheme [20].

As a result of the studies mentioned above, these newly observed excited Ω_b states can be viewed as P -wave states. In quark models, the Ω_b states have three valence quarks, ssb . If we don't include an additional P -wave to this system, we can obtain the ground states of Ω_b as $\Omega_b(J^P = \frac{1}{2}^+)$ and $\Omega_b(J^P = \frac{3}{2}^+)$. For the time being, only the $\Omega_b(\frac{1}{2}^+)$ is observed [21]. But if there exist a relative P -wave between two s -quarks or between ss diquark and b quark, seven negative parity Ω_b states can be obtained. Furthermore, if this relative P -wave excitation takes about an energy of 300-500 MeV, then P -wave Ω_b states have the mass in the range of 6300-6400 MeV. Quark models and diquark-quark models finds similar mass values [22, 23].

In the present work, we will study Ω_b^- states in quark model via artificial neural network. In Section II, Hypercentral Constituent Quark Model (hCQM) is presented. Section III is devoted to the Artificial Neural Network and application of it to quantum mechanical systems. In Section IV, we present our results for mass spectrum,

*Electronic address: halilmutuk@gmail.com

radiative and strong decay widths comparing with available experimental data and theoretical studies. A short summary is concluded in the last section.

II. QUARK MODEL OF Ω_b^- STATE

A baryon is an example of quantum mechanical version of classical three-body system. Three-quark systems with a heavy quark (Q) of mass m_Q and two light quarks (qq) of equal mass m_q can be studied in this prescribed way. Single heavy baryons with one heavy quark (Q) (c or b) and two light quarks (u , d and s) provide a laboratory for studying the dynamics of the light quarks in the presence of a heavy quark. Two states which are in the same mode but have different spin numbers may mix in the heavy quark limit since light-quark spin-spin force is still on work in this limit.

In this present work, we use non-relativistic framework of hypercentral Constituent Quark Model (hCQM) which is well established for the study of the properties of baryons [24–28].

A. Hypercentral Constituent Quark Model (hCQM)

The fundamental idea of the hypercentral approach to three-body systems is simple. The coordinates of the bodies in the system are rewritten in terms of the relative coordinates. In this case, two relative coordinates ($\vec{\rho}$, $\vec{\lambda}$) are rewritten into a non-relativistic Schrödinger equation in the six-dimensional space. The hyperradius x and hyperangle ξ is given as

$$x = \sqrt{\vec{\rho}^2 + \vec{\lambda}^2}, \quad \xi = \arctan \frac{\rho}{\lambda}. \quad (5)$$

To remove the center of mass motion of the system, Jacobi coordinates can be used [26]

$$\vec{\rho} = \frac{1}{\sqrt{2}}(\vec{r}_1 - \vec{r}_2), \quad (6)$$

$$\vec{\lambda} = \frac{m_1\vec{r}_1 + m_2\vec{r}_2 - (m_1 + m_2)\vec{r}_3}{m_1^2 + m_2^2 + (m_1 + m_2)^2}, \quad (7)$$

where r_i and $m_i = (1, 2, 3)$ denote the spatial and the mass coordinate of the i -th constitute quark. The reduced mass corresponding to Jacobi coordinates $\vec{\rho}$ and $\vec{\lambda}$ are

$$m_\rho = \frac{2m_1m_2}{m_1 + m_2}, \quad (8)$$

$$m_\lambda = \frac{2m_3(m_1^2 + m_2^2 + m_1m_2)}{(m_1 + m_2)(m_1 + m_2 + m_3)}, \quad (9)$$

where $m_i = (1, 2, 3)$ are the constituent quark masses. The angles of the hyperspherical coordinates are given by $\Omega_\rho = (\theta_\rho, \phi_\rho)$ and $\Omega_\lambda = (\theta_\lambda, \phi_\lambda)$.

After having removed the center of mass motion by using Jacobi coordinates, the kinetic energy operator can be written as

$$\begin{aligned} \frac{P_x^2}{2m} &= -\frac{\hbar^2}{2m}(\Delta_\rho + \Delta_\lambda) \\ &= -\frac{\hbar^2}{2m} \left(\frac{\partial^2}{\partial x^2} + \frac{5}{x} \frac{\partial}{\partial x} + \frac{L^2(\Omega)}{x^2} \right) \end{aligned} \quad (10)$$

where $m = \frac{2m_\rho m_\lambda}{m_\rho + m_\lambda}$ is the reduced mass and $L^2(\Omega) = L^2(\Omega_\rho, \Omega_\lambda, \xi)$ is the six dimensional generalization of the squared angular momentum operator and is a representation of quadratic Casimir operator of the six-dimensional rotational group $O(6)$. Its eigenfunctions are the hyperspherical harmonics $Y_{[\gamma]l_\rho l_\lambda}(\Omega_\rho, \Omega_\lambda, \xi)$ satisfying the eigenvalue relation

$$L^2 Y_{[\gamma]l_\rho l_\lambda}(\Omega_\rho, \Omega_\lambda, \xi) = -\gamma(\gamma+4) Y_{[\gamma]l_\rho l_\lambda}(\Omega_\rho, \Omega_\lambda, \xi). \quad (11)$$

Here $\vec{L} = \vec{L}_\rho + \vec{L}_\lambda$, l_ρ and l_λ are the angular momenta associated with the Jacobi coordinates ($\vec{\rho}$, $\vec{\lambda}$) and γ is the hyperangular momentum quantum number satisfying $\gamma = 2n + l_\rho + l_\lambda$ where n is a nonnegative integer. Notice that in the hCQM, it is hard to separate ρ - mode excitations and λ - mode excitations since the sets ($l_\rho = 1, l_\lambda = 0$) which is ρ - mode excitation and ($l_\rho = 0, l_\lambda = 1$) which is λ - mode excitation give the same hyperangular momentum quantum number, γ .

The potential for the hCQM can be written in terms of hyperradius (x) as

$$\sum_{i<j} V(r_{ij}) = V(x) + \dots \quad (12)$$

In this approximation, the three-quark potential is a function of only the hyperradius x and the dependence on the single pair coordinates cannot be disentangled from the third one. Therefore it contains not only two-body interactions but also contains three-body interactions. The case of three-body interactions are important in the study of hadrons since the existence of a direct gluon-gluon interaction-which is the non-abelian feature of QCD- produce three-body forces.

The potential is a key ingredient in the study of meson and baryon spectra. In the present study, we consider the hypercentral potential $V(x)$ as the hyper Coulomb plus linear potential with second order correction and spin-dependent interaction, which is given as follows [29]:

$$V(x) = V^0(x) + \left(\frac{1}{m_\rho} + \frac{1}{m_\lambda} \right) V^1(x) + V^2(x) + V_{SD}(x), \quad (13)$$

where $V^0(x)$ is given by

$$V^0(x) = \frac{\tau}{x} + \beta x, \quad (14)$$

where $\tau = -\frac{2}{3}\alpha_s$ is the hyper Coulomb strength corresponding to the strong running coupling constant α_s and β is the string tension of the confinement part.

The first-order correction reads as:

$$V^{(1)}(x) = -C_F C_A \frac{\alpha_s^2}{4x^2}, \quad (15)$$

where, C_F and C_A are the casimir charges of the fundamental and adjoint representation and α_s is the strong running coupling constant.

The second-order correction is given by (with the notation of $m = \frac{2m_\rho m_\lambda}{m_\rho + m_\lambda}$) [30]:

$$\begin{aligned} V^2(x) &= -\frac{C_F D_{1,s}^{(2)}}{2m^2} \left\{ \frac{1}{x} \cdot \vec{p}^2 \right\} + \frac{C_F D_{2,s}^{(2)}}{2m^2} \frac{1}{x^3} \vec{L}^2 \\ &+ \frac{\pi C_F D_{d,s}^{(2)}}{m^2} \delta^{(3)}(\vec{x}) + \frac{4\pi C_F D_{S^2,s}^{(2)}}{3m^2} \vec{S}^2 \delta^{(3)}(\vec{x}) \\ &+ \frac{3C_F D_{LS,s}^{(2)}}{2m^2} \frac{1}{x^3} \vec{L} \cdot \vec{S} \\ &+ \frac{C_F D_{S_{12},s}^{(2)}}{4m^2} \frac{1}{x^3} S_{12}(\hat{x}), \end{aligned} \quad (16)$$

where $S_{12}(\vec{r}) \equiv 3\hat{x} \cdot \vec{\sigma}_1 \hat{x} \cdot \vec{\sigma}_2 - \vec{\sigma}_1 - \vec{\sigma}_2$ and $\vec{S} = \vec{\sigma}_1/2 + \vec{\sigma}_2/2$.

In order to obtain the expressions for the coefficients, one has to perform the matching between nonrelativistic QCD (NRQCD) and potential nonrelativistic QCD (pNRQCD). A procedure for this matching can be found in [31, 32]. After matching, one can obtain the relevant contributions as follows [30]:

$$\begin{aligned} \delta D_{1,s}^{(2)} &= \alpha_s(x), \\ \delta D_{2,s}^{(2)} &= \alpha_s(x), \\ \delta D_{d,s}^{(2)} &\simeq \alpha_s(x) \left\{ 1 + \frac{\alpha_s}{\pi} \left(\frac{2C_F}{3} + \frac{17C_A}{3} \right) \ln mx \right\}, \\ \delta D_{S^2,s}^{(2)} &\simeq \alpha_s(x) \left\{ 1 - \frac{7C_A}{4} \frac{\alpha_s}{\pi} \ln mx \right\}, \\ \delta D_{LS,s}^{(2)} &\simeq \alpha_s(x) \left\{ 1 - \frac{2C_A}{3} \frac{\alpha_s}{\pi} \ln mx \right\}, \\ \delta D_{S_{12},s}^{(2)} &\simeq \alpha_s(x) \left\{ 1 - C_A \frac{\alpha_s}{\pi} \ln mx \right\}. \end{aligned} \quad (17)$$

One interesting point here is that, spin-dependent potentials do not have $\ln mx$ contributions. The spin-dependent part of the potential reads as follows:

$$\begin{aligned} V_{SD}(x) &= V_{SS}(\vec{S}_\rho \cdot \vec{S}_\rho) + V_{\gamma S}(x)(\vec{\gamma} \cdot \vec{S}) \\ &+ V_T(x) \left[S^2 - \frac{3(\vec{S} \cdot \vec{x})(\vec{S} \cdot \vec{x})}{x^2} \right], \end{aligned} \quad (18)$$

where, $\vec{S} = \vec{S}_\rho + \vec{S}_\lambda$ with \vec{S}_ρ is the spin vector of $\vec{\rho}$ and \vec{S}_λ is the spin vector of $\vec{\lambda}$.

The spin dependent potential contains three types of the interaction: the spin-spin term V_{SS} which gives spin

singlet triplet splittings, the spin-orbit term $V_{\gamma S}$ and tensor term V_T give the fine structure of the states [33]. Defining $V_V(x) = \frac{\tau}{x}$ as vector part and $V_S(x) = \beta x$ as scalar part of the static potential, these spin-dependent terms can be written as follows:

$$V_{SS}(x) = \frac{1}{3m_\rho m_\lambda} \nabla^2 V_V, \quad (19)$$

$$V_{\gamma S}(x) = \frac{1}{2m_\rho m_\lambda x} \left(3 \frac{dV_v}{dx} - \frac{dV_s}{dx} \right), \quad (20)$$

$$V_T(x) = \frac{1}{6m_\rho m_\lambda} \left(3 \frac{d^2 V_v}{dx^2} - \frac{1}{x} \frac{dV_v}{dx} \right). \quad (21)$$

The Hamiltonian of the three-quark system in the hQCM can be written as

$$H = \frac{P_x^2}{2m} + V(x), \quad (22)$$

where $m = \frac{2m_\rho m_\lambda}{m_\rho + m_\lambda}$ is the reduced mass and x is the six-dimensional radial hypercentral coordinate of the three-quark system. After writing the Hamiltonian the next step is solving Schrödinger equation, $H\Psi = E\Psi$.

In conventional quark model, Schrödinger equation is solved in three-dimensional space. In hQCM, Schrödinger equation lives in six-dimensional space and needs to be handled. This can be done in conventional way such as numerically. In this work, we have solved six-dimensional Schrödinger equation by using Artificial Neural Networks, (ANNs). There are some advantages of using ANN for solving differential equations [34]

- Computational complexity does not increase quickly in the ANN method when the number of sampling points is increased while in the other standard numerical methods computational complexity increases rapidly as the number of sampling points increased in the interval
- Model based on neural network offers an opportunity to tackle in real time difficult differential equation problems arising in many sciences and engineering applications.
- The ANN method to solve a differential equation provides a solution with very good generalization properties.

The main advantage of using ANN is that computational complexity does not increase considerably when the number of dimensions in problem increase. The other point is that the solution is continuous overall the domain of integration.

III. FORMALISM OF ARTIFICIAL NEURAL NETWORK

Especially the last decade has seen a significant raise of interest in machine learning where the learning part is

done by the artificial neural networks. Artificial neural networks (ANNs) are systems of simple processing elements (called "neurons") managing their data and communicating with other elements.

The fundamental ingredient of an artificial neural network is neuron (perceptron in computerized systems). Figure 1 represents a single artificial neuron.

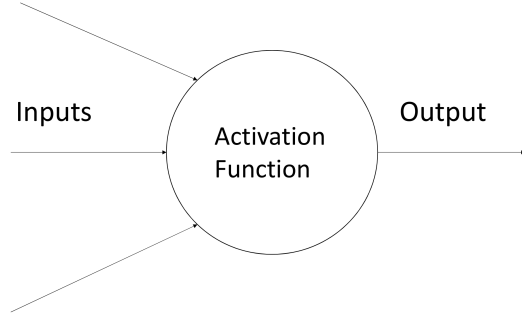


FIG. 1: A model of single neuron

Each neuron receives any number of input and produces only one output. If this output comes from input layers, it will be an input for the hidden layers. In this manner, the inputs are the outputs of activation functions in where the inputs are multiplied by the connection weights. This activation function (neuron transfer function) determines the output. In practice, one single neuron is not capable of handling problems. That's why networks composed of neurons are being used. In Figure 2, the architecture of a multilayer perceptron is shown.

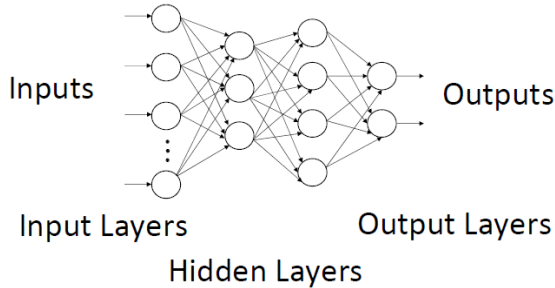


FIG. 2: Multilayer neural network

The most common architecture of ANNs is the multilayer feed forward network. In this study, we consider a feed forward neural network with one input layer, one

hidden layer and one output layer. The signals are propagated from the input layer to the output layer where each processing element is responsible for operating the signals coming from preceding layer and sending information to the connected next layer. Fig. 1 is an example of feed forward neural network.

A. Mathematical Model of an Artificial Neural Network

The relationship of the input and output of the network layers can be written as follows:

$$o_i = \sigma(n_i), \quad (23)$$

$$o_j = \sigma(n_j), \quad (24)$$

$$o_k = \sigma(n_k), \quad (25)$$

where i is for input, j is for hidden and k is for output layers. Input to the neurons read as

$$n_i = (\text{Input signal to the NN}), \quad (26)$$

$$n_j = \sum_{i=1}^{N_i} \omega_{ij} o_i + \theta_j, \quad (27)$$

$$n_k = \sum_{i=1}^{N_j} \omega_{jk} o_j + \theta_k, \quad (28)$$

where, N_i and N_j are the numbers of units in the input and hidden layers, ω_{ij} is the synaptic weight parameter which connects the neurons i and j and θ_j and θ_k are the threshold parameters of the neurons j and k , respectively [35]. The output of the network defined as

$$o_k = \sum_{j=1}^{b_n} \omega_{jk} \sigma \left(\sum_{i=1}^{a_n} \omega_{ij} n_i + \theta_j \right) + \theta_k. \quad (29)$$

One needs derivative of above function since it will be used in evaluation of error function. This can be obtained as

$$\frac{\partial o_k}{\partial \omega_{ij}} = \omega_{jk} \sigma^{(1)}(n_j) n_i, \quad (30)$$

$$\frac{\partial o_k}{\partial \omega_{jk}} = \sigma(n_j) \delta_{kk'}, \quad (31)$$

$$\frac{\partial o_k}{\partial \theta_j} = \omega_{jk} \sigma^{(1)}(n_j), \quad (32)$$

$$\frac{\partial o_k}{\partial \theta_k} = \delta_{kk'}. \quad (33)$$

Activation function of a neuron defines the output of that neuron for given an input or inputs. In this work, sigmoid function

$$\sigma(x) = \frac{1}{1 + e^{-x}} \quad (34)$$

is used as an activation function. This function is continuous in everywhere and belongs to class C^∞ . Therefore, it is possible to derive all the derivatives of $\sigma(x)$. This is an important aspect for the Schrödinger equation since it is a second order differential equation.

B. Application to Quantum Mechanics

Consider the following differential equation

$$H\Psi(x) = f(x). \quad (35)$$

Here H is a linear operator, $f(x)$ is a known function and $\Psi(x) = 0$ at the boundaries. A general method for solving this equation is to try a function which is believed to be a solution. For this reason, a trial function such as

$$\Psi_t(\mathbf{x}) = A(\mathbf{x}) + B(\mathbf{x}, \eta)N(\mathbf{x}, \mathbf{p}) \quad (36)$$

can be written. This trial function depends on \mathbf{p} and η which are to be neural network parameters. \mathbf{p} is the weight and bias of the artificial neural network. In Eq. 36, $A(\mathbf{x})$ and $B(\mathbf{x}, \eta)$ should be adjusted so that $\Psi_t(\mathbf{x})$ satisfies boundary conditions of the given equation. In order to solve Eq. (35), collocation method can be used. In this method, one choose a finite-dimensional space for trial solutions and a number of points in the domain. After doing that, given differential equation can be transformed into a minimization problem

$$\min_{p, \eta} \sum_i [H\Psi_t(x_i) - f(x_i)]^2. \quad (37)$$

In terms of eigenvalue equation, Eqn. (35) takes the form

$$H\Psi(x) = \epsilon\Psi(x), \quad (38)$$

where $\Psi(x)$ satisfies the boundary condition, $\Psi(x) = 0$. In this case, the trial solution can be written as

$$\Psi_t(x) = B(\mathbf{x}, \eta)N(\mathbf{x}, \mathbf{p}). \quad (39)$$

Here, $B(\mathbf{x}, \eta) = 0$ at boundary conditions for a range of η values. If we discretize the domain of the problem, which is a part of collocation method, Schrödinger equation can be transformed into a minimization problem, as mentioned before:

$$E(\mathbf{p}, \eta) = \frac{\sum_i [H\Psi_t(x_i, \mathbf{p}, \eta) - \epsilon\Psi_t(x_i, \mathbf{p}, \eta)]^2}{\int |\Psi_t|^2 d\mathbf{x}}. \quad (40)$$

Here E is the error function and ϵ can be computed as

$$\epsilon = \frac{\int \Psi_t^* H\Psi_t d\mathbf{x}}{\int |\Psi_t|^2 d\mathbf{x}}. \quad (41)$$

For further details of application of neural networks to quantum mechanical problems, see Ref. [36].

The three-quark wave function can be factorized as

$$\psi_{3q}(\vec{\rho}, \vec{\lambda}) = \psi_{\gamma\nu}(x)Y_{[\gamma]l_\rho l_\lambda}(\Omega_\rho, \Omega_\lambda, \xi). \quad (42)$$

Here, hyperradial wave function $\psi_{\gamma\nu}(x)$ is labeled by the grand angular quantum number γ and by the number of nodes ν . The angular-hyperangular part of the $3q$ -state is completely described by the hyperharmonics and is same for any hypercentral potential. The dynamics is contained in the hyperradial wave function [26]:

$$\psi_{\gamma\nu}(x) = \left[\frac{v!(2g)^6}{(2g+2\nu+5)(\nu+2\gamma+4)!^3} \right]^{1/2} \cdot (2gx)^\gamma e^{-gx} L_\nu^{2\gamma+4}(2gx), \quad (43)$$

where $g = \frac{\tau m}{\gamma + \nu + 5/2}$.

Then, the hyperradial Schrödinger equation can be written as follows:

$$\left[\frac{d^2}{dx^2} + \frac{5}{x} \frac{d}{dx} - \frac{\gamma(\gamma+4)}{x^2} \right] \psi_{\gamma\nu}(x) = -2m[E - V(x)] \psi_{\gamma\nu}(x). \quad (44)$$

We used a trial wave function as

$$\psi_t(x) = x^{5/2} \psi_{\gamma\nu}(x) N(x, u, w, v), \quad (45)$$

with N being a feed forward neural network with one hidden layer and m sigmoid hidden units

$$N(x, u, w, v) = \sum_{j=1}^m v_j \sigma(w_j x + u_j). \quad (46)$$

To obtain desired results, the first thing that ANN has to do is learning. The learning mechanism is the most important property of ANN. In this work, we used a feed forward neural network with a back propagation algorithm which is also known as delta learning rule. This learning rule is valid for continuous activation function, such as Eqn. 34. The algorithm is as follows [37]:

- Step 1 Initialize the weights w from the input layer to the hidden layer and weights v from the hidden layer to the output layer. Choose the learning parameter (lies between 0 and 1) and error E_{max} . Initially error is taken as 0.
- Step 2 Train the network.
- Step 3 Compute the error value.
- Step 4 Compute the error signal terms of the output layer and the hidden layer.
- Step 5 Compute components of error gradient vectors.
- Step 6 Check the weights if they are properly modified.
- Step 7 If $E = E_{max}$ terminate the training session. If not, go to step 2 with $E \rightarrow 0$ and initiate a new training.

The main point to train the network is to initialize the eigenvalue (E) (error function) is to zero and train the network with 150 equidistance points in the interval after selecting one hidden unit. The aim is to get energy

function to be zero or at least tends to be zero. If the convergence is not achieved, then the eigenvalue would be wrong. In that case, eigenvalue should be changed and tried again. If the error function value did not converge to zero after doing these steps, the number of the hidden units must be changed (increased) and run a new cycle. We keep doing this until the error function converges to zero.

By employing this approach it is possible to obtain energy eigenvalues of the Schrödinger equation. We trained the network with some equidistance points in the intervals with $m = 5$ and solved the Schrödinger equation in the interval $0 < x < 1$ with $\psi(0) = 0$ at the boundaries. We did not analyze the number of hidden units in the present paper. The optimum value was obtained after doing some calculations.

IV. NUMERICAL RESULTS AND DISCUSSION

The numerical parameters and constants used in this work are

$$\begin{aligned}
m_s &= 0.500 \text{ GeV}, \\
m_b &= 4.67 \text{ GeV}, \\
C_F &= 2/3, \\
C_A &= 3, \\
n_f &= 3, \\
\alpha_s &= 0.6 \ (\mu_0 = 1 \text{ GeV}), \\
\tau &= -0.4 \\
\beta &= 0.18
\end{aligned}$$

The comparison of the obtained mass spectra with other quark models is shown in Table I with the spectroscopic notation ($n^{2s+1}L_j$) except L (angular momentum quantum number) is replaced by γ (hyper-angular momentum quantum number) in hCQM.

It can be seen from Table I that the obtained mass values are in good agreement with the other theoretical studies. The LHCb collaboration observed four narrow structures of excited Ω_b^- states, namely $\Omega_b^-(6316)$, $\Omega_b^-(6330)$, $\Omega_b^-(6340)$ and $\Omega_b^-(6350)$ in the $\Xi_b^0 K^-$ mass spectrum. The theory predicts five states whereas experiment observed only four states. The remaining state should have a broad width which can hardly be observed in experiments. The quantum numbers of newly observed excited Ω_b^- states are not available. Some recent efforts are done and the results can be seen in Table 2.

TABLE II: J^{PC} quantum number assignments to the excited Ω_b^- states of recent studies.

State	[16]	[17]	[19]
$\Omega_b^-(6316)$	$\frac{1}{2}^-$ or $\frac{3}{2}^-$	$\frac{1}{2}^-$	$\frac{3}{2}^-$
$\Omega_b^-(6330)$	$\frac{1}{2}^-$	$\frac{3}{2}^-$	$\frac{1}{2}^-$
$\Omega_b^-(6340)$	$\frac{3}{2}^-$	$\frac{3}{2}^-$	$\frac{5}{2}^-$
$\Omega_b^-(6350)$	$\frac{3}{2}^-$ partner with $\frac{5}{2}^-$	$\frac{5}{2}^-$	$\frac{3}{2}^-$

Since there is no available data upto now on quantum numbers of these excited states, there is no possibility to rule out them.

A. Radiative Decays of Excited Ω_b^- States

The study of electromagnetic transitions of baryons is an important issue for understanding the internal structure of baryons. To calculate the partial widths of the E1 radiative transitions of the ($n^{2s+1}L_j \rightarrow n'^{2s'+1}L'_j + \gamma$) process, we use [38]:

$$\Gamma_{E_1} = \frac{4}{3} C_{fi} \delta_{ss'} e_q^2 \alpha |\langle R_f | r | R_i \rangle|^2 E_\gamma^3 \quad (47)$$

where e_q is the quark charge, α is the fine-structure constant, E_γ is the final photon energy. The matrix element C_{fi} is given as

$$C_{fi} = \max(L, L') (2J' + 1) \begin{Bmatrix} L' & S' & J \\ J & L & 1 \end{Bmatrix}. \quad (48)$$

In order to calculate matrix elements, we need $\langle R_f | r | R_i \rangle$, where R represents the radial wave function of the meson. In this work, we generalize radial wave function to hyperradial wave function, r to hyper radius x , L (angular momentum quantum number) is replaced by γ (hyper-angular momentum quantum number), and meson mass to the baryon mass. For the masses of the initial and final states, we used our calculated values. Apart from hCQM, this generalization from meson to baryon electromagnetic transitions were successfully done in [39, 40]. The matrix elements of $\langle R_f | r | R_i \rangle$ were calculated in ANN framework by setting suitable quantum numbers for initial and final states hyperradial wave functions, $\psi_{\gamma\nu}(x)$. In Table III, we present the partial widths of the radiative decays of excited Ω_b^- baryons. Our predictions are compatible with the result of Ref. [24]. Radiative decays of $1^2P_{1/2}$ and $1^2P_{3/2}$ to $\Omega_b\gamma$ and $1^4P_{3/2}$ and $1^4P_{3/2}$ to $\Omega_b^*\gamma$ are very different than others. If these decays are studied in further experiments, this situation can be identified.

TABLE I: Comparison of mass values of excited Ω_b^- states with other quark models. Results are in MeV.

State	This Work	RQM [5]	NQM [6]	hCQM [14]	QM [23]
$1^2P_{1/2}$	6314	6330	6333	6338	6305 ± 15
$1^2P_{3/2}$	6330	6331	6336	6328	6317 ± 19
$1^4P_{1/2}$	6339	6339	6340	6343	6313 ± 15
$1^4P_{3/2}$	6342	6340	6344	6333	6325 ± 19
$1^4P_{5/2}$	6352	6334	6345	6320	6338 ± 20

TABLE III: Partial widths for the radiative decays of the excited Ω_b^- states. Results are in keV.

State	$\Gamma[\Omega_b\gamma]$		$\Gamma[\Omega_b^*\gamma]$	
	This work	[46]	This work	[46]
$1^2P_{1/2}$	138	154	1.41	1.49
$1^2P_{3/2}$	71.8	83.4	1.45	1.51
$1^4P_{1/2}$	0.85	0.64	104.29	99.23
$1^4P_{3/2}$	2.03	1.81	73.65	70.68
$1^4P_{5/2}$	1.02	1.21	51.57	63.26

B. Decay Widths of Excited Ω_b^- States

Besides the mass prediction, the investigation of other physical properties such as radiative decays of the considered resonances would be helpful to identify these resonances more reliably. The study of strong decay of these resonances is also helpful in this respect. The study of the strong decay processes is a challenge task both theoretically and experimentally.

In this work, we adopt the 3P_0 model [41–44] to calculate the two-body strong decay widths of the low-lying Ω_b states. This model is an efficient model to compute open-flavor strong decays of hadrons in the quark model framework. In this model a hadron decay occurs in its rest frame and proceeds via the creation of an additional $q\bar{q}$ pair. This quark-antiquark pair is created with vacuum quantum numbers, $J^{PC} = 0^{++}$. The decay widths can be computed by

$$\Gamma_{A \rightarrow BC} = \frac{2\pi\gamma_0^2}{2J_A + 1} \Phi_{A \rightarrow BC}(q_0) \sum_{M_{J_A}, M_{J_B}} |\mathcal{M}^{M_{J_A}, M_{J_B}}|^2. \quad (49)$$

Here, $|\mathcal{M}^{M_{J_A}, M_{J_B}}|$ is the $A \rightarrow BC$ amplitude, γ_0 is the dimensionless pair creation strength, q_0 is the relative momentum between B and C . The coefficient $\Phi_{A \rightarrow BC}(q_0)$ is the phase space factor for the decay. The nonrelativistic expression for this factor reads as

$$\Phi_{A \rightarrow BC}(q_0) = 2\pi q_0 \frac{M_b M_c}{M_A}. \quad (50)$$

The baryon wave function is chosen as $\psi_{3q}(\vec{p}, \vec{\lambda}) = \psi_{11}(x) Y_{[1]} l_0 l_1$. The free parameter (pair creation strength) γ_0 is taken as 9.3. For the wave function and other issues please see Refs. [23, 45]. In the bottom baryon systems, the heavy quark symmetry should

be preserved quite well, that is, the light quark spin $\vec{j} = \vec{s}_1 + \vec{s}_2 + \vec{L}$ is an approximate good quantum number rather than the total spin $\vec{S} = \vec{s}_1 + \vec{s}_2 + \vec{s}_3$. The physical resonances should correspond to the mixing of the states in the $L - S$ coupling scheme adopted in this work. The mixing of the states with same J^P is taken into account for the strong decay decay behaviours. The obtained decay widths are given in Table IV.

TABLE IV: Strong decay widths of $\Gamma(\Omega_b \rightarrow \Xi_b K^-)$. Results are in MeV.

State	This work	[23]	[46]
$1^2P_{1/2}$	0.64	0.50	49.53
$1^2P_{3/2}$	2.97	2.79	1.90
$1^4P_{1/2}$	1.52	1.14	95.08
$1^4P_{3/2}$	0.46	0.62	0.29
$1^4P_{5/2}$	2.62	4.28	1.66

As can be seen from Table IV, our results are in good agreement with Ref. [23] and compatible with Ref. [46]. The discrepancy in two results for the states of $1^2P_{1/2}$ and $1^2P_{3/2}$ of Ref. [46] is interesting. Regarding the strong decays for baryon states, no satisfactory model has been achieved. So the reason for this discrepancy may be as a result of non-existence of a single model for explaining baryon open-flavor strong decays.

V. SUMMARY AND CONCLUDING REMARKS

In this paper, we have employed hypercentral constituent quark model to compute mass spectra by solving six-dimensional Schrödinger equation by using artificial neural network. The obtained mass spectra are in good agreement with other works. Given the uncertainties of different quark models predictions, these structures are good candidates of the $\Omega_b(1P)$ states. As mentioned before, there are five states for Ω_b in the quark model. Since there are only four observed Ω_b states and one is remaining, the status and fate of remaining state is still unclear.

We also obtained radiative decay of excited Ω_b^- states by generalizing the method given in Ref. [38]. The results are appealing for this generalization and we hope this can be used in further studies. The radiative decay widths for Ω_b^- states is in compatible with the reference study.

Within the results of radiative decays, $1^2P_{1/2}$ and $1^2P_{3/2}$ to $\Omega_b\gamma$ and $1^4P_{1/2}$ and $1^2P_{3/2}$ to $\Omega_b^*\gamma$ are very large than the others.

Strong decay widths are calculated via a generalization of 3P_0 model. Obtained results are in good agreement with available experimental data and theoretical studies.

The results for $1^2P_{1/2}$ and $1^4P_{1/2}$ of Ref. [46] are roughly order of magnitude larger than our results.

We hope future experiments on radiative and strong decay widths of excited Ω_b^- states will clarify the spin assignments and the status of the missing state which have not been observed yet.

-
- [1] R. Aaij et al. [LHCb Collaboration], First observation of excited Ω_b^- states, arXiv:2001.00851 [hep-ex].
- [2] H. Garcilazo, J. Vijande and A. Valcarce, Faddeev study of heavy baryon spectroscopy, J. Phys. G **34**, 961 (2007), arXiv:hep-ph/0703257.
- [3] D. Ebert, R. N. Faustov and V. O. Galkin, Masses of excited heavy baryons in the relativistic quark model, Phys. Lett. B **659**, 612 (2008), arXiv:0705.2957 [hep-ph].
- [4] W. Roberts and M. Pervin, Heavy baryons in a quark model, Int. J. Mod. Phys. A **23**, 2817 (2008), arXiv:0711.2492 [nucl-th].
- [5] D. Ebert, R. N. Faustov and V. O. Galkin, Spectroscopy and Regge trajectories of heavy baryons in the relativistic quark-diquark picture, Phys. Rev. D **84**, 014025 (2011), arXiv:1105.0583 [hep-ph].
- [6] T. Yoshida, E. Hiyama, A. Hosaka, M. Oka and K. Sadato, Spectrum of heavy baryons in the quark model, Phys. Rev. D **92**, 114029 (2015).
- [7] G. Yang, J. Ping and J. Segovia, The S- and P-Wave Low-Lying Baryons in the Chiral Quark Model, Few Body Syst. **59**, 113 (2018), arXiv:1709.09315 [hep-ph].
- [8] Q. Mao, H. X. Chen, W. Chen, A. Hosaka, X. Liu and S. L. Zhu, QCD sum rule calculation for P-wave bottom baryons, Phys. Rev. D **92**, 114007 (2015), arXiv:1510.05267 [hep-ph].
- [9] S. S. Agaev, K. Azizi and H. Sundu, Decay widths of the excited Ω_b baryons, Phys. Rev. D **96**, 094011 (2017), arXiv:1708.07348 [hep-ph].
- [10] H. M. Yang, H. X. Chen, E. L. Cui, A. Hosaka and Q. Mao, arXiv:1909.13575 [hep-ph].
- [11] S. S. Agaev, K. Azizi and H. Sundu, On the nature of the newly discovered Ω states, EPL **118**, 61001 (2017), arXiv:1703.07091 [hep-ph].
- [12] X.-W. Kang, J. A. Oller, Eur. Phys. J. C **77** 399 (2017), arXiv:1612.08420 [hep-ph].
- [13] D. Ebert, R. N. Faustov and V. O. Galkin, Spectroscopy and Regge trajectories of heavy baryons in the relativistic quark-diquark picture, Phys. Rev. D **84**, 014025 (2011), arXiv:1105.0583 [hep-ph].
- [14] K. Thakkar, Z. Shah, A. K. Rai and P. C. Vinodkumar, Excited State Mass spectra and Regge trajectories of Bottom Baryons, Nucl. Phys. A **965**, 57 (2017), arXiv:1610.00411 [nucl-th].
- [15] K. W. Wei, B. Chen, N. Liu, Q. Q. Wang and X. H. Guo, Spectroscopy of singly, doubly, and triply bottom baryons, Phys. Rev. D **95**, 116005 (2017), arXiv:1609.02512 [hep-ph].
- [16] H. X. Chen, E. L. Cui, A. Hosaka, Q. Mao and H. M. Yang, Excited Ω_b baryons and fine structure of strong interaction, arXiv:2001.02147 [hep-ph].
- [17] W. Liang and Q. F. Lü, Strong decays of the newly observed narrow Ω_b structures, arXiv:2001.02221 [hep-ph].
- [18] W. H. Liang and E. Oset, The observed Ω_b spectrum and meson-baryon molecular states, arXiv:2001.02929 [hep-ph].
- [19] Z.G. Wang, Analysis of the $\Omega_b(6316)^-$, $\Omega_b(6330)^-$, $\Omega_b(6340)^-$ and $\Omega_b(6350)^-$ within QCD Sum Rules, arXiv:2001.02961 [hep-ph].
- [20] L.Y. Xiao, K.L. Wang, M.S. Liu, X.H. Zhong, Possible interpretation of the newly observed Ω_b states, arXiv:2001.05110 [hep-ph].
- [21] M. Tanabashi et al. (Particle Data Group), Phys. Rev. D **98**, 030001 (2018).
- [22] Z. G. Wang, Analysis of the $\frac{1}{2}^-$ and $\frac{3}{2}^-$ heavy and doubly heavy baryon states with QCD sum rules, Eur. Phys. J. A **47**, 81 (2011), arXiv:1003.2838 [hep-ph].
- [23] E. Santopinto, A. Giachino, J. Ferretti, H. Garcia-Tecocoatzi, M. A. Bedolla, R. Bijker and E. Ortiz-Pacheco, The Ω_c -puzzle solved by means of quark model predictions, Eur. Phys. J. C **79**, 1012 (2019), arXiv:1811.01799 [hep-ph].
- [24] Z. Ghahani and A. Rajabi, S.-x. Qin and D.H. Rischke, Ground-state masses and magnetic moments of heavy baryons, Mod. Phys. Lett. A **29**(20), 1450106, (2014), arXiv:1403.4582 [hep-ph].
- [25] E. Santopinto, Interacting quark-diquark model of baryons, Phys. Rev. C **72**, 022201 (2005), arXiv:hep-ph/0412319.
- [26] M. M. Giannini, E. Santopinto, The hypercentral Constituent Quark Model and its application to baryon properties, Chin. J. Phys. **53**, 020301 (2015), arXiv:1501.03722 [nucl-th].
- [27] Z. Shah, K. Thakkar, A.K. Rai, Excited state mass spectra of doubly heavy baryons Ω_{cc} , Ω_{bb} , and Ω_{bc} , Eur. Phys. J. C **76**, 530 (2016), arXiv:1609.03030 [hep-ph].
- [28] J. Ballot and M. Fabre de la Ripelle, Applications of Hyperspherical Formalism to the Trinucleon Bound State Problems, Ann. of Phys. (N.Y.) **127**, 62 (1980).
- [29] Y. Koma, M. Koma, and H. Wittig, Nonperturbative Determination of the QCD Potential at $O(1/m)$, Phys. Rev. Lett. **97**, 122003 (2006), arXiv:hep-lat/0607009.
- [30] N. Brambilla, A. Pineda, J. Soto, and A. Vairo, The Heavy Quarkonium Spectrum at Order $m\alpha_s^5 \ln \alpha_s$, Phys. Lett. B **470**, 215-222 (1999), arXiv:hep-ph/9910238.
- [31] N. Brambilla, A. Pineda, J. Soto, A. Vairo, Potential NRQCD: an effective theory for heavy quarkonium, Nucl. Phys. B **566**(1-2), 275-310, arXiv:hep-ph/9907240.
- [32] A. Pineda and J. Soto, Potential NRQED: The positronium case, Phys. Rev. D **59**, 016005 (1999), arXiv:hep-ph/9805424.
- [33] M.B. Voloshin, Charmonium, Prog. Part. Nucl. Phys. **61**, 455-511 (2008), arXiv:0711.4556 [hep-ph].
- [34] N. Yadav, A. Yadav, M. Kumar, An Introduction to Neural Network Methods for Differential Equations, Springer in Applied Sciences and Technology, (2015); D. R. Parisi, M. C. Mariani, M. A. Laborde, Solving differential equa-

- tions with unsupervised neural networks, Chem. Eng. Process. **42**, 715-721 (2003).
- [35] M. Sugawara, Numerical solution of the Schrödinger equation by neural network and genetic algorithm, Comput. Phys. Commun. **140**, 366-380 (2001).
- [36] I.E. Lagaris, A. Likas, D.I. Fotiadis, Artificial Neural Network Methods in Quantum Mechanics, Comput. Phys. Commun. **104**, 1-14 (1997), arXiv:9705029 [quant-ph].
- [37] J. M. Zurada, Introduction to Artificial Neural Systems, West Publishing Co., St. Paul, MN, (1992).
- [38] E. Eichten, K. Gottfried, T. Kinoshita, K. D. Lane, and T. M. Yan, Charmonium: The Model, Phys. Rev. D **17** 3090, (1978).
- [39] W. J. Deng, H. Liu, L. C. Gui and X. H. Zhong, Spectrum and electromagnetic transitions of bottomonium, Phys. Rev. D **95**, 074002 (2017), arXiv:1607.04696 [hep-ph].
- [40] W. J. Deng, H. Liu, L. C. Gui and X. H. Zhong, Charmonium spectrum and their electromagnetic transitions with higher multipole contributions, Phys. Rev. D **95**, 034026 (2017), arXiv:1608.00287 [hep-ph].
- [41] L. Micu, Decay rates of meson resonances in a quark model, Nucl. Phys. B **10**, 521 (1969).
- [42] A. Le Yaouanc, L. Oliver, O. Pene and J.-C. Raynal, Naive quark pair creation model of strong interaction vertices, Phys. Rev. D **8**, 2223 (1973).
- [43] R. Bijker, J. Ferretti, G. Galata, H. Garcia-Tecocoatz and E. Santopinto, Strong decays of hadrons and missing resonances, Phys. Rev. D **94**, 074040 (2016), arXiv:1506.07469 [hep-ph].
- [44] T. Barnes, S. Godfrey and E. S. Swanson, Higher charmonia, Phys. Rev. D **72**, 054026 (2005), arXiv:hep-ph/0505002.
- [45] E. Santopinto, F. Iachello, M.M. Giannini, Nucleon form factors in a simple three-body quark model, Eur. Phys. J. A **1**, 307-315 (1998),
- [46] K. L. Wang, Y. X. Yao, Z. H. Zhong, and Q. Zhao, Strong and radiative decays of the low-lying $S-$ and $P-$ wave singly heavy baryons, Phys. Rev. D **96**, 116016 (2017) arXiv:1709.04268 [hep-ph].